In Vivo Imaging of Human Cerebral Nicotinic Acetylcholine Receptors with 2-^{18}F-Fluoro-A-85380 and PET

Jean-Dominique Gallezot, MS[1]; Michel Bottlaender, MD, PhD[1]; Marie-Claude Grégoire, PhD[2]; Dimitri Roumenov, MD[1]; Jean-Robert Deverre, PhD[1]; Christine Coulon, BS[1]; Michèle Ottaviani, BS[1]; Frédéric Dollé, PhD[1]; André Syrota, MD, PhD[1]; and Héric Valette, MD[1]

[1]Service Hospitalier Frédéric Joliot, Departement de Recherche Medicale/Direction des Sciences du Vivant, Commissariat à l'Energie Atomique, Orsay, France; and [2]Unité de Recherche Associée Commissariat à l'Energie Atomique-Centre National de la Recherche Scientifique 2210, Service Hospitalier Frédéric Joliot, Orsay, France

2-^{18}F-Fluoro-3-[2(*S*)-2-azetidinylmethoxy]pyridine (2-^{18}F-fluoro-A-85380) is a PET radioligand that is specific for nicotinic acetylcholine receptors (nAChRs) and has a high affinity for the $\alpha_4\beta_2$ subtype. The purpose of this study was to evaluate different strategies to quantify 2-^{18}F-fluoro-A-85380 binding in healthy nonsmoking human volunteers. **Methods:** After intravenous injection of 189 ± 30 MBq (0.8–5.7 nmol) of 2-^{18}F-fluoro-A-85380, the first dynamic PET scan was acquired over 150 min. The second 30-min PET scan was performed 60 min later. Time–activity curves were generated from volumes of interest. 2-^{18}F-Fluoro-A-85380 volume of distribution (DV) was quantified using compartmental kinetic analysis and Logan graphical analysis. In the kinetic analysis, the 1-tissue compartment model (1TCM) and the 2-tissue (2TCM) compartment model were applied. The most appropriate kinetic model was determined using the Akaike Information Criterion. The effect of reducing the PET study duration on the reliability of the DV values computed by the kinetic and the graphical analyses was evaluated. **Results:** Time–activity curves were better described by the 2TCM. The DV values ranged from 5.2 ± 0.5 in the occipital cortex, 6.2 ± 0.2 in the frontal cortex, and 7.3 ± 0.4 in the putamen to 15.4 ± 2.1 in the thalamus. These regional DV values were consistent with the distribution of nAChRs in the human brain. Logan graphical analysis provided slightly lower DV values than those of the 2TCM (from −3.5% in the occipital cortex to −6.6% in the thalamus). The minimal study duration required to obtain stable DV estimates in all regions was similar for the 2 methods: 140 min for the 2TCM and 150 min for the Logan analysis. DV estimates obtained with the 2TCM were more stable than those calculated by the Logan approach for the same scan duration. **Conclusion:** These results show that 2-^{18}F-fluoro-A-85380 can be used to assess nAChRs binding in the human brain with PET.

Key Words: 2-^{18}F-fluoro-A-85380; PET; nicotinic receptors; human brain; distribution volume

J Nucl Med 2005; 46:240–247

The nicotinic acetylcholine neurotransmitter system plays a crucial role in the mediation of memory learning, neuropsychiatric diseases, drug addiction, and control of pain (*1*). Degeneration of cells expressing nicotinic receptors (nicotinic acetylcholine receptors [nAChRs]) has been observed in several neurodegenerative diseases, including Parkinson's and Alzheimer's diseases (*2*).

Imaging of nAChRs using PET could provide useful information on the integrity of this system in vivo. For example, in view of the projected doubling of the incidence of Alzheimer's disease cases every 20 y (*3*), noninvasive imaging of nAChRs could have an important impact on public health, since it can be a potentially valuable technique for the diagnosis and follow-up of these patients. Although nAChRs are among the best-studied receptors in vitro, potentially useful PET and SPECT ligands were developed only recently. They are halogenate derivatives of the A-85380 (3-[2(*S*)-2-azetidinylmethoxy]pyridine): 2-^{18}F-fluoro-A-85380 (2-fluoro-3-[2(*S*)-2-azetidinylmethoxy-]pyridine) (*4–7*), 6-^{18}F-fluoro-A-85380 (*4,7*), and 5-^{123}I-iodo-A-85380 (*4,7*). Previously, ^{11}C-nicotine has been used, but this compound has several drawbacks (*8*). 2-^{18}F-Fluoro-A-85380 is an $\alpha_4\beta_2$ subtype–selective nicotinic cholinergic agonist, which has been characterized in rodents and baboons (*5,6,9*). Its acute toxicity is low compared with that of epibatidine derivatives (*5,10*). In the course of phase I studies, a previous investigation was undertaken to assess the whole-body biodistribution of 2-^{18}F-fluoro-A-85380 and to calculate the associated radiation-absorbed doses in healthy human volunteers. This study demonstrated the possibility of imaging nAChRs in healthy volunteers using a maximal dose of 258 MBq (*11*). Moreover, 2-fluoro-A-85380 demonstrated no mutagenic properties (*12*).

As part of phase II studies, the present investigation aimed at assessing the brain distribution of 2-^{18}F-fluoro-A-85380 in healthy volunteers. To quantify 2-^{18}F-fluoro-A-85380 regional cerebral distribution volumes (DVs), 2 methods were compared: compartmental kinetic modeling

Received Jun. 29, 2004; revision accepted Sep. 24, 2004.

For correspondence or reprints contact: Héric Valette, MD, Service Hospitalier Frédéric Joliot, Departement de Recherche Medicale/Direction des Sciences du Vivant, Commissariat à l'Energie Atomique, 4 Place du Général Leclerc, F-91406 Orsay, France.

E-mail: valette@shfj.cea.fr

and Logan graphical analysis (*13*). Due to the slow kinetics of the ligand, which is a drawback for its use in patients, the effect of reducing the study duration was also evaluated for each method to determine the shortest PET scan duration providing reliable results.

MATERIALS AND METHODS

Radiopharmaceutical

2-Fluoro-A-85380 was labeled with the positron emitter ^{18}F by no-carrier-added nucleophilic aromatic substitution by the $K^{18}F$–$F\text{-}K_{222}$ complex with (3-[2(*S*)-*N*-(*t*-butoxycarbonyl)-2-azetidinylmethoxy]pyridin-2-yl)trimethylammonium trifluoromethanesulfonate (where *t*-butoxycarbonyl is Boc) as a highly efficient labeling precursor, followed by trifluoroacetic acid removal of the Boc protective group (*6*). The total synthesis time was 50–55 min from the end of the cyclotron ^{18}F production. Radiochemical yields, with respect to initial ^{18}F-fluoride ion radioactivity, were 68%–72% (decay corrected). The specific radioactivities at the end of the synthesis were 148–222 GBq/μmol.

Subjects

The Medical Bioethics Committee of the Medical Centre at the University of Paris XI approved this study. Seven healthy male volunteers, with a mean age of 27.7 y (range, 23–37 y) and a mean weight of 71.7 kg (range, 54–92 kg) gave their written informed consent for participation in the study. The subjects were free of medical illness on the basis of screening by medical history, physical examination, serum chemical analysis, complete blood cell count, and urine analysis. All were nonsmokers, as demonstrated by the negative plasma cotinine determination. A standard 12-lead electrocardiogram was obtained for screening purposes. Serum chemical analysis, complete blood cell count, and urine analysis were performed before and within a week after completion of the PET study.

Experimental Protocols

Each subject underwent 1 PET scan and 1 T1-weighted MR scan, the latter to identify anatomic brain regions.

PET Procedures

PET experiments were performed with a CTI HR+ Exact positron tomograph (CPS Innovations). This scanner allows simultaneous acquisition in 3-dimensional (3D) mode of 63 slices with an isotropic intrinsic resolution of 4.5 mm (*14*). The subjects were in the supine position, with the head in the middle of the field of view of the camera. The head was maintained using a molded thermoplastic mask. A transmission scan was acquired for 15 min using 3 retractable ^{68}Ge rod sources. 2-^{18}F-Fluoro-A-85380 was then intravenously injected (189 ± 30 MBq, 0.8–5.7 nmol) as a 1-min bolus and the emission scan was started. A dynamic series was acquired with sampling times of 1 × 20 s, 10 × 10 s, 3 × 20 s, 3 × 1 min, 2 × 2 min, 10 × 3 min, 16 × 5 min, and 3 × 10 min for a total acquisition of 150 min. The subjects were then removed from the gantry and repositioned in the PET scanner 60 min later. The second dynamic series consisted of three 10-min images followed by an acquisition of a second short transmission scan (5 min). The first dynamic images were corrected for attenuation using the transmission scan data acquired before the injection. For the second dynamic series, attenuation correction was performed using the final transmission scan data, after segmentation of the attenuation map (*15*). The first 2 subjects had a single acquisition that lasted 120 min.

Arterial Blood Sampling

During the PET acquisition, 33 arterial blood samples (1 mL each) were withdrawn from the radial artery at designated times. Blood and plasma radioactivities were measured in a cross-calibrated γ-counter (Cobra Quantum D5003; Perkin-Elmer), and the activity was corrected for ^{18}F decay from the time of the injection.

Metabolite High-Performance Liquid Chromatography (HPLC) Analysis

For each subject, 4 arterial blood samples (3 mL) were withdrawn from the radial artery at different times. Plasma analysis was performed by HPLC as previously described (*5*).

The fraction of unchanged 2-^{18}F-fluoro-A-85380 was quantified using a calibration curve. In a preliminary experiment, the yield of the whole plasma analysis process (including protein precipitation using acetonitrile, acetonitrile evaporation, HPLC run, and radioactivity detection) was measured over a concentration range of 2-^{18}F-fluoro-A-85380 (dissolved in human plasma) from 70 to 4,700 Bq/mL.

A control measurement was performed for each subject: Arterial plasma was withdrawn before the PET scan, 2-^{18}F-fluoro-A-85380 was added to this plasma at 1–3 different concentrations (1,900–5,900 Bq/mL), and these samples (thereafter referred to as control samples) were injected in the HPLC loop to check the system stability.

Then, for each sample obtained after injection of 2-^{18}F-fluoro-A-85380, the total plasma radioactivity was measured with a γ-counter (as described). The radioactivity due to unchanged 2-^{18}F-fluoro-A-85380, obtained after elution of the HPLC column and quantified using the calibration curve, was expressed as a fraction of the total plasma radioactivity.

MRI

Each subject was submitted to an MR scan on a 1.5-T Signa system (General Electric Medical Systems). A T1-weighted inversion-recovery sequence in 3D mode and a 256 × 192 matrix over 124 slices (1.5-mm thick) was used to generate the anatomic images.

Regions of Interest (ROIs)

Nine volumes of interest (VOIs) were delineated in 3 dimensions on MR T1 images, based on clearly identified anatomic structures: frontal (8.8 ± 2.4 mL), parietal (7.5 ± 2.0 mL), temporal (5.8 ± 0.8 mL), and occipital (15.9 ± 4.0 mL) cortices, caudate nucleus (3.3 ± 0.5 mL), putamen (4.0 ± 0.8 mL), thalamus (7.5 ± 1.0 mL), cerebellum (15.0 ± 3.7 mL), and hippocampus (1.8 ± 0.4 mL).

Brain Time–Activity Curves

To ensure the consistency of the anatomic localization of 2-^{18}F-fluoro-A-85380 cerebral binding, coregistration of PET images to the corresponding MR images was performed using a mutual information algorithm (*16*). The mean radioactivity in the VOIs was calculated for each frame, and time–activity curves were plotted versus time.

For the second dynamic series, the bias on the regional radioactivity (RA) values induced by segmenting the attenuation map was corrected with the following procedure. The first transmission image was also segmented and the last 3 frames of the first

dynamic series were reconstructed using either the segmented (RA_{seg}) or the measured (RA_{meas}) attenuation map. The bias induced by using the segmented transmission was estimated in each VOI as:

$$BIAS_{VOI} = (RA_{seg} - RA_{meas})/RA_{meas}. \quad \text{Eq. 1}$$

Then, the corrected regional activities (RA_{corr}) obtained with the second dynamic series were computed as:

$$RA_{corr} = RA_{seg}/(1 + BIAS_{VOI}). \quad \text{Eq. 2}$$

PET Data Kinetic Analysis

For kinetic analysis, 2 compartmental models were tested: the 1-tissue compartment (1TCM) and the 2-tissue compartment (2TCM) models (Fig. 1). In the latter, we assume that the concentration of free (unbound) ligand and the concentration of nonspecifically bound ligand equilibrate rapidly compared with PET acquisition times. The compartments in the 2TCM correspond to the radioactivity concentrations of unchanged radioligand in plasma (C_P), free or nonspecifically bound radioligand in brain (C_{F+NS}), and radioligand specifically bound to receptor sites (C_B). The rate constants K_1 and k_2 describe the influx and efflux rates, respectively, through the blood–brain barrier. The rate constants k_3 and k_4 describe the radioligand transfer between the free (and nonspecifically bound) compartment and the specific binding compartment. The differential equations of the 2TCM are given by:

$$\begin{aligned} dC_{F+NS}(t)/dt &= K_1C_P(t) - (k_2 + k_3)C_{F+NS}(t) + k_4C_B(t), \\ dC_B(t)/dt &= k_3C_{F+NS}(t) - k_4C_B(t), \\ C_{TISSUE}(t) &= C_{F+NS}(t) + C_B(t), \end{aligned} \quad \text{Eq. 3}$$

where C_{TISSUE} is the PET radioactivity concentration in the cerebral VOI measured by PET and corrected for the radioactivity due to the cerebral blood volume (assumed to be 5%) (*17*). The system is linear since the radioligand is injected at a tracer dose. The total DV (DV_{2TCM}) has the advantage of being more stable than the kinetic parameters (K_1, k_2, k_3, and k_4) determined individually (*18*). It can be expressed in terms of the kinetic rate parameters as follows:

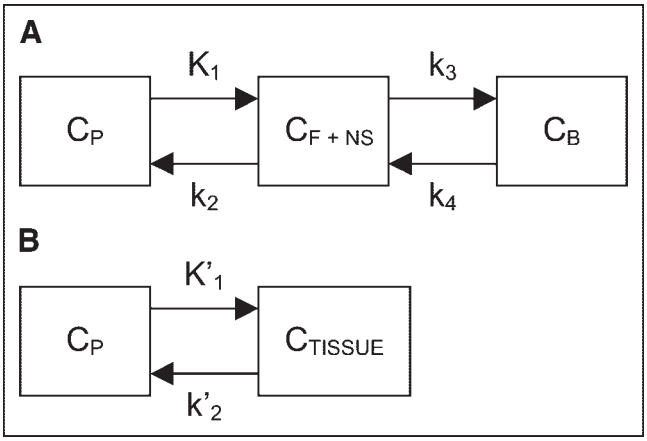

FIGURE 1. 1TCM and 2TCM. (A) Compartments in 2TCM correspond to radioactivity concentrations of unchanged radioligand in plasma (C_P), free or nonspecifically bound radioligand in brain (C_{F+NS}), and radioligand specifically bound to receptors sites (C_B). (B) In 1TCM, single-tissue compartment corresponds to total tissue radioactivity (C_{TISSUE}).

$$DV_{2TCM} = K_1/k_2 \times (1 + k_3/k_4). \quad \text{Eq. 4}$$

In the 1TCM, we additionally assume that the concentrations C_{F+NS} and C_B equilibrate rapidly and, therefore, can be combined into a single compartment. The rate constants were denoted K'_1 and k'_2 to avoid confusion with the 2TCM. The total DV for the 1TCM is noted as DV_{1TCM} and is given by:

$$DV_{1TCM} = K'_1/k'_2. \quad \text{Eq. 5}$$

Weighted nonlinear least-square fitting was performed using the Marquardt algorithm (*19*) to identify the 4 and 2 parameters of the 2TCM or of the 1TCM, respectively. Goodness of fit was evaluated using the χ^2 criterion. Model relevancy was assessed using the Akaike Information Criterion (AIC) (*20*). The most appropriate model provides the smallest AIC. To evaluate the kinetic parameter identifiability, the coefficient of variation of the parameter given by the diagonal of the covariance matrix (*21*) was computed and expressed as percentage of the parameter estimate (%COV).

Logan Graphical Analysis

The graphical approach (*13*) for the analysis of reversible radioligand kinetics was also applied to the present data. This method allows one to measure the total DV of the ligand without any assumption on the actual configuration of the tissue compartment(s). Assuming 2 tissue compartments and that C_B and C_{TISSUE} equilibrate for $t > T_0$, the operational equation is:

$$\frac{\int_0^T C_{TISSUE}(t)dt}{C_{TISSUE}(T)} = \left[\frac{K_1}{k_2}\left(1 + \frac{k_3}{k_4}\right)\right]\frac{\int_0^T C_P(t)dt}{C_{TISSUE}(T)} + R. \qquad T > T_0 \quad \text{Eq. 6}$$

The slope of the linear section of the plot of $\int_0^T C_{TISSUE}(t)dt/C_{TISSUE}(T)$ versus $\int_0^T C_P(t)dt/C_{TISSUE}(T)$ is the total DV, thereafter-referred to as DV_{Logan}. DV_{Logan} was computed by linear regression of the final part of the plot, after a time T_0 fixed to a common value for all VOIs and subjects.

Effect of PET Study Duration on DV Values

Due to the slow kinetics of 2-^{18}F-fluoro-A-85380, the DV values obtained with a 4-h PET acquisition were considered as a priori reference values. To investigate the effect of reducing the scan duration on the DV values, the kinetic analysis and the graphical analysis were performed with scan durations ranging from 90 to 150 min with 10-min increments. For each method and duration T, relative bias values were expressed as $(DV_T - DV_{4hour})/DV_{4hour}$. Two criteria were used to define the minimum acceptable study duration for each quantification method: (a) the mean bias had to be <5% and (b) the maximal bias had to be <10% in all VOIs.

Software

Anatomist software (http://brainvisa.free.fr) was used for VOI drawing, PET–MRI coregistration, and time–activity curve computations. The kinetic modeling and Logan graphical analysis were performed with the Pmod Software (http://www.pmod.com). The statistic tests were performed with Statview (SAS).

RESULTS

Biosafety

After injection of an average of 189 MBq 2-^{18}F-fluoro-A-85380 (range, 161–237 MBq; range, 0.77–5.66 nmol), no adverse or subjective effects were noted in any of the

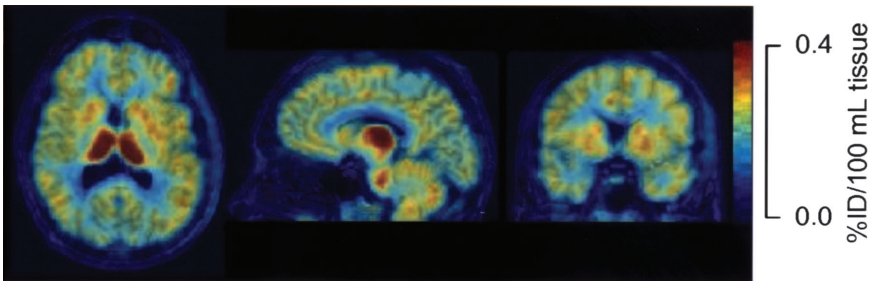

FIGURE 2. Axial, sagittal, and coronal mean PET images (from left to right) obtained between 60 and 120 min in 1 subject, after injection of 2-^{18}F-fluoro-A-85380 (174 MBq). PET images are represented with coregistered MR images. %ID = percentage injected dose.

subjects. Their vital signs remained stable throughout the experiment. No meaningful changes were observed in any of the clinical laboratory assays performed on the blood and urine specimens obtained before and after administration of the radioligand (data not shown).

Brain and Plasma Time–Activity Curves

Typical images obtained after injection of 2-^{18}F-fluoro-A-85380 in 1 subject are shown in Figure 2. Characteristic brain time–activity curves are shown in Figure 3. As expected, the highest cerebral concentration of ligand (percentage injected dose [%ID]) was observed in the thalamus, where the maximal concentration was 0.46 ± 0.07 %ID/100 mL tissue. Intermediate levels were observed in the putamen (0.32 ± 0.05 %ID/100 mL tissue), cerebellum (0.31 ± 0.04 %ID/100 mL tissue), and cortex (0.27 ± 0.04 %ID/100 mL tissue). The lowest concentration was observed in the white matter (0.19 ± 0.03 %ID/100 mL tissue).

The kinetics of 2-^{18}F-fluoro-A-85380 were slow. In the cortical regions, the average concentration peak time ranged between 43 ± 12 min (occipital) and 69 ± 11 min (temporal). In the basal ganglia and cerebellum, the concentration peaked at 65 ± 10 min and 56 ± 6 min, respectively. The fastest washout occurred in the occipital cortex. Conversely, in the thalamus, the maximal concentration could not always be observed during the 240 min of the experient.

In arterial plasma, the clearance of the total radioactivity can be fitted by the sum of 3 exponential functions with a late half-life (the slowest of the exponential functions) of approximately 6 h (Fig. 4).

The ratio between the concentration of radioactivity in the tissue and the concentration of unchanged 2-^{18}F-fluoro-A-85380 in the plasma (tissue-to-plasma ratio) stabilized very slowly in all VOIs, except in the thalamus, where no equilibrium was reached over the experimental time interval.

HPLC Analysis

The calibration experiment showed that the 2-^{18}F-fluoro-A-85380 HPLC peak area and the activity measured with

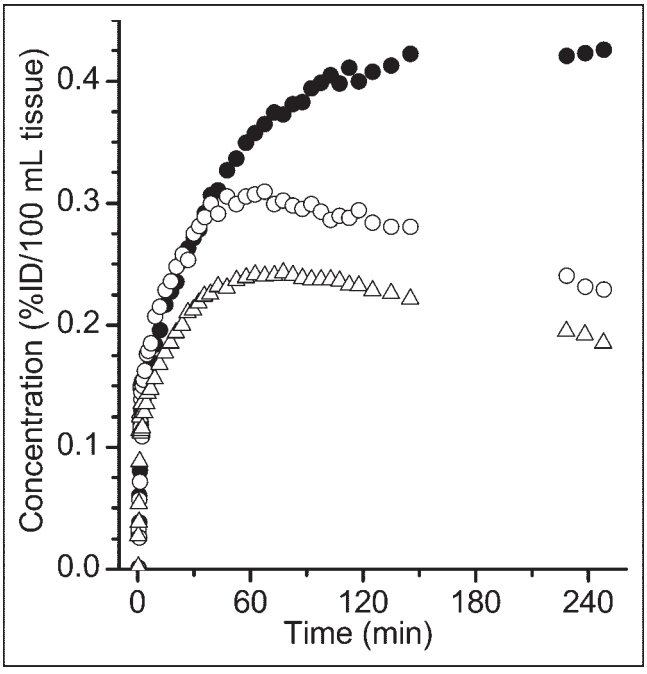

FIGURE 3. Representative time–activity curves obtained after injection of 2-^{18}F-fluoro-A-85380 in 1 healthy subject in thalamus (●), putamen (○), and temporal cortex (△).

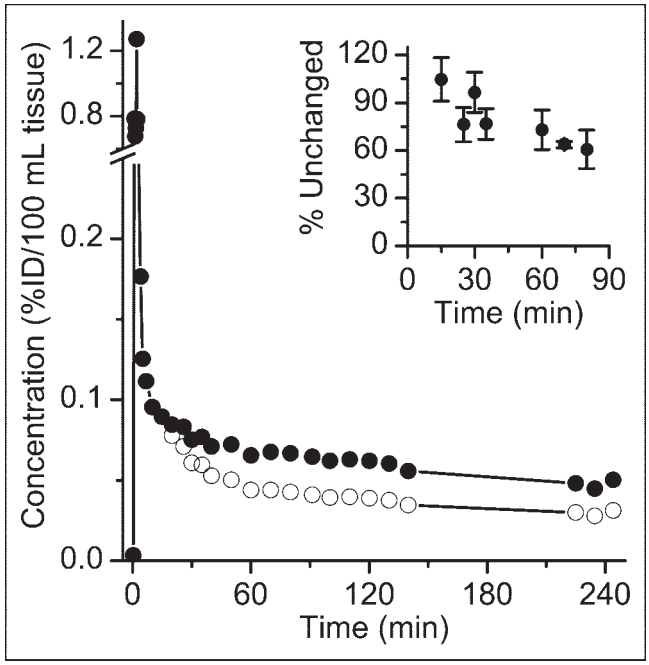

FIGURE 4. Concentration of total radioactivity in plasma (●) and concentration of unchanged 2-^{18}F-fluoro-A-85380 (○) vs. time. (Inset) Time course of percentage of radioactivity in plasma corresponding to unchanged 2-^{18}F-fluoro-A-85380 (●, mean ± SD, n = 7).

TABLE 1
Comparison of χ^2 Criterion, AIC, and DV Values for 1TCM and 2TCM ($n = 5$)

Region	χ^2 criterion		AIC		DV	
	1TCM	2TCM	1TCM	2TCM	1TCM	2TCM
Caudate	1.02 ± 0.26	0.87 ± 0.17	203 ± 11	200 ± 9	6.37 ± 0.18	6.59 ± 0.32
Putamen	1.10 ± 0.40	0.98 ± 0.39*	204 ± 20	203 ± 27	7.10 ± 0.39	7.27 ± 0.41*
Thalamus	0.81 ± 0.16	0.37 ± 0.16*	191 ± 10	153 ± 22*	14.8 ± 1.89	15.4 ± 2.18*
Cerebellum	1.55 ± 1.12	0.59 ± 0.38*	215 ± 36	171 ± 30*	6.75 ± 0.42	7.03 ± 0.44*
Hippocampus	6.26 ± 1.67	1.42 ± 0.37*	295 ± 13	224 ± 17*	5.62 ± 0.40	6.23 ± 0.60*
Frontal cortex	0.65 ± 0.33	0.36 ± 0.29*	176 ± 24	143 ± 34*	6.07 ± 0.19	6.20 ± 0.19*
Parietal cortex	0.87 ± 0.42	0.45 ± 0.24*	190 ± 28	158 ± 35*	5.54 ± 0.14	5.71 ± 0.24*
Occipital cortex	3.23 ± 0.90	1.03 ± 0.10*	261 ± 14	209 ± 11*	5.02 ± 0.39	5.16 ± 0.49*
Temporal cortex	0.65 ± 0.22	0.49 ± 0.34	178 ± 20	160 ± 33	5.81 ± 0.40	5.91 ± 0.45*

*Difference between the 2 models is statistically significant ($P < 0.05$ Student paired t test).
DV values are expressed in mL plasma/mL tissue. Values are presented as mean ± SD.

the γ-counter were significantly correlated ($r = 0.996$, $P < 0.001$, $n = 10$). The numeric values of the control samples were not significantly different from the calibration curve (analysis of covariance [ANCOVA], $P = 0.17$; test for homogeneity of regression, $P = 0.09$). Therefore, the same regression equation was used to convert the HPLC peak area to the radioactivity value for all samples. The mean curve of the fraction of unchanged 2-^{18}F-fluoro-A-85380 in arterial plasma is presented in the inset of Figure 4.

Kinetic Analysis

The χ^2 criterion, AIC, and DV values obtained with the 1TCM and the 2TCM are presented in Table 1. For both criteria, the values were statistically lower for the 2TCM (repeated-measures ANOVA, $P < 0.001$ for both AIC and χ^2 criterion). Ad hoc paired Student t tests performed in each region showed that both the χ^2 criterion and AIC differences were statistically significant in all VOIs, except in the caudate nucleus, putamen, and temporal cortex. The 1TCM parameters K'_1 and k'_2 were well identified in all VOIs, with %COV values close to 1% and 3%, respectively. As expected, the 2TCM kinetic parameters k_2, k_3, and k_4 were poorly identified in all regions. SDs for the DV_{2TCM} and DV_{1TCM} were not significantly different in any VOI (F test, $P = 0.39$, lower regional P value). Finally, according to the AIC, the 2TCM was selected in all VOIs. One can notice that the DV_{1TCM} values were systematically lower than the DV_{2TCM} values.

Logan Graphical Analysis

Characteristic Logan plots obtained in 1 subject are shown in Figure 5, and DV_{Logan} estimates are presented in Table 2. DV_{Logan} values were significantly lower than the DV_{2TCM} values (repeated-measures ANOVA, $P < 0.001$). The mean difference ranged from −3.5% in the occipital cortex to −6.6% in the thalamus (overall mean = −5.0%). The variance of the 2 estimates DV_{2TCM} and DV_{Logan} was not significantly different (F test, $P = 0.71$, lower regional P value).

Effect of PET Study Duration on DV Estimates

The effect of reducing the PET study duration on the DV value was investigated using the 4-h DV estimates as reference values (Fig. 6). The thalamus was excluded from this analysis, because no washout phase could be observed during the 4 h of the experiment in most subjects; therefore, the 4-h DV estimates could not be used as reference values in this structure.

In the kinetic analysis, both selection criteria for the minimum study duration (mean bias <5% and maximal bias <10%) were satisfied if the study duration was ≥130 min in most VOIs. A 140-min study duration was necessary

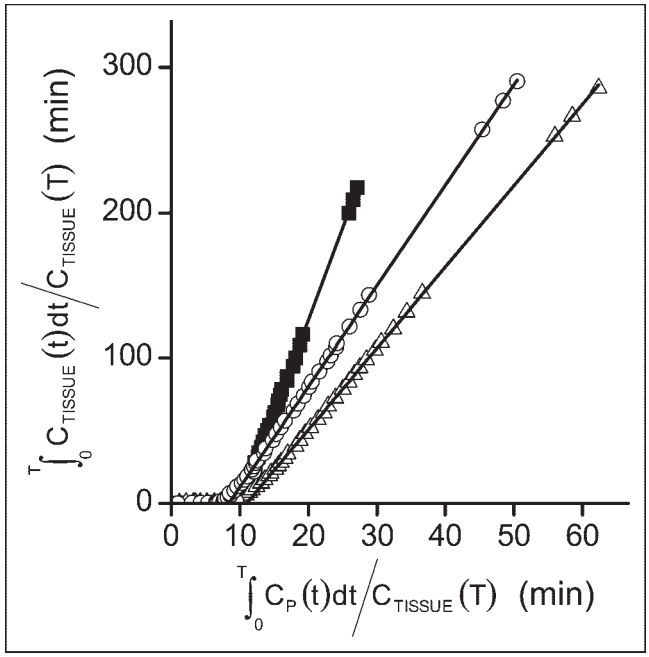

FIGURE 5. Representative Logan plots in 1 healthy subject in thalamus (■), putamen (○), and temporal cortex (△). For each region, symbols correspond to experimental measured values; straight lines correspond to regression curves.

TABLE 2
DV Values for Kinetic and Graphical Analyses Determined from 4-Hour Studies (n = 5)

Region	Logan plot	Kinetic analysis*
Caudate	6.25 ± 0.30	6.59 ± 0.32
Putamen	6.89 ± 0.41	7.27 ± 0.41
Thalamus	14.41 ± 1.98	15.43 ± 2.18
Cerebellum	6.74 ± 0.49	7.03 ± 0.44
Hippocampus	5.97 ± 0.56	6.23 ± 0.60
Frontal cortex	5.88 ± 0.24	6.20 ± 0.19
Parietal cortex	5.42 ± 0.30	5.71 ± 0.24
Occipital cortex	4.98 ± 0.42	5.16 ± 0.49
Temporal cortex	5.58 ± 0.45	5.91 ± 0.45

*In kinetic analysis, the 2TCM was used in all regions.
DV values are expressed in mL plasma/mL tissue. Values are presented as mean ± SD.

to keep the mean bias <5% in the temporal cortex. Reducing the study duration had little effect on the criteria used to select the most appropriate compartmental model: For every study duration tested, the AIC values of the 2TCM were lower than those of the 1TCM in all VOIs.

With the Logan analysis, both selection criteria were satisfied if the study duration was ≥120 min in most VOIs. However, a 150-min study duration was required to fulfill the 2 criteria in the hippocampus.

For a 140-min scan duration, the SD of the bias was lower with the kinetic analysis compared with the Logan analysis (−24% in average for all VOIs) (Table 3).

DISCUSSION

The aim of this study was to assess the regional distribution of 2-^{18}F-fluoro-A-85380 in the human brain and to determine the optimal PET study duration.

The regional distribution of 2-^{18}F-fluoro-A-85380 DV was consistent with known densities of nAChRs in the human brain. PET regional distribution of 2-^{18}F-fluoro-A-85380 could be compared with the densities determined in vitro (measured either on autoradiographic slices or on membrane preparations) using reference ligands. ^{3}H-Nicotine demonstrated a more heterogeneous distribution of binding sites (*22,23*) than that of 2-^{18}F-fluoro-A-85380. On the contrary, ^{3}H-epibatidine (*23*) and 2-^{18}F-fluoro-A-85380 showed a more homogeneous distribution: Only the thalamus displays the highest binding and the other cerebral structures have a rather homogeneous density. Among the extrathalamic regions, using ^{3}H-epibatidine in vitro, the caudate nucleus, putamen, and cerebellum showed the highest receptor density, followed by the cortex and, finally, the hippocampus. With 2-^{18}F-fluoro-A-85380, the rank order was the same, except for the hippocampus, whose DV was higher than that of the cortical ROIs. Several factors could explain this difference. First, the limited resolution of PET can induce a spillover effect from surrounding areas, especially the external parts of the thalamus. Second, this difference could also be due to the age difference between the subjects in the 2 studies (77.2 ± 7.7 y (*22*)). Thus, ^{3}H-epibatidine and 2-^{18}F-fluoro-A-85380 exhibit very close distribution profiles in the human brain.

The brain kinetics of 2-^{18}F-fluoro-A-85380 were similar to those of ^{123}I-5I-A-85380 measured by SPECT (*24*). The

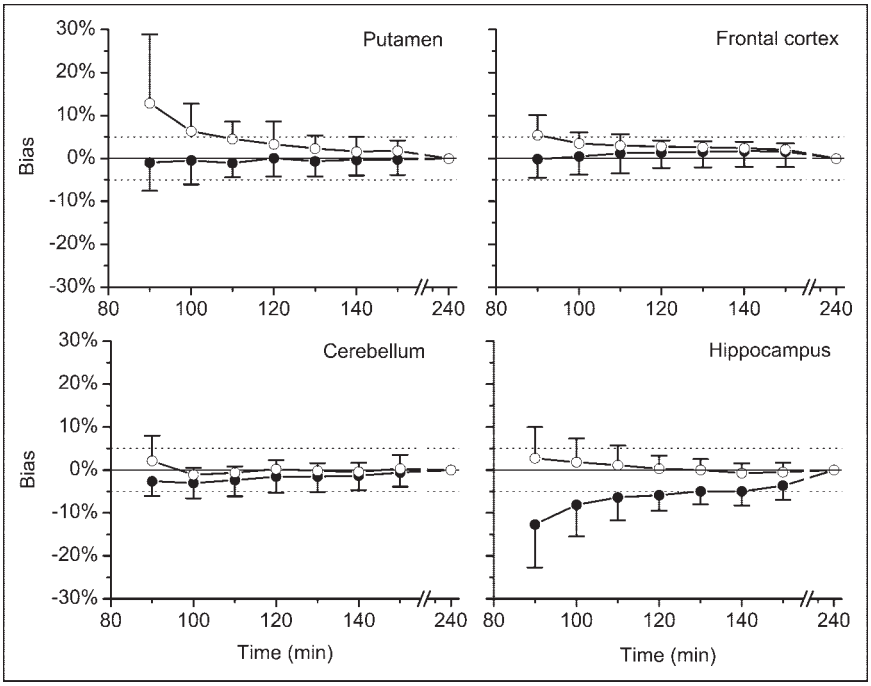

FIGURE 6. Effect of study duration on stability of DV_{Logan} (●, lower error bar) and DV_{2TCM} (○, upper error bar) values in 4 VOIs. Values are presented as mean ± SD (n = 5). For putamen, 1 DV_{2TCM} value was excluded at 90 and 100 min.

TABLE 3
Relative Bias (%) on DV Values for 140-Minute Study Compared with 4-Hour Reference Values ($n = 5$)

Region	2TCM (kinetic analysis)	Logan (graphical analysis)
Caudate	−1.1 ± 4.0	−3.3 ± 2.7
Putamen	1.6 ± 2.4	−0.3 ± 3.6
Cerebellum	−0.4 ± 3.2	−1.3 ± 3.2
Hippocampus	−0.7 ± 2.2	−4.6 ± 3.7
Frontal cortex	2.3 ± 1.4	1.6 ± 3.8
Parietal cortex	1.5 ± 2.3	0.5 ± 4.9
Occipital cortex	0.8 ± 2.0	1.8 ± 3.5
Temporal cortex	5.0 ± 2.4	3.4 ± 3.1

Values are presented as mean ± SD.

maximal concentration value of 2-^{18}F-fluoro-A-85380 was about 50% of that of ^{123}I-5I-A-85380 in all regions and the DV values were 3.3 times lower. These differences could be explained by the higher lipophilicity and higher affinity for the $\alpha_4\beta_2$ subtype of the iodinated compound. The regional distribution of the DV values for 2-^{18}F-fluoro-A-85380 and ^{123}I-5I-A-85380 are highly correlated ($r = 0.995$, $P < 0.001$, $n = 7$). 2-^{18}F-Fluoro-A-85380 maximal concentrations and DV values are similar (10% lower) and highly correlated ($r = 0.997$, $P < 0.001$, $n = 7$) with those of 6-^{18}F-fluoro-A-85380 (*25*). Both 6-^{18}F-fluoro-A-85380 and ^{123}I-5I-A-85380 displayed a slightly faster kinetics than that of 2-^{18}F-fluoro-A-85380, especially in the thalamus. This difference could be explained by the relative hydrophilicity of the 3 compounds. This faster kinetics allows a more reliable quantification of the thalamic DV values.

Due to the low concentration of nAChRs in the brain and the high affinity of 2-^{18}F-fluoro-A-85380 for the $\alpha_4\beta_2$ nicotinic subtype, the injected dose should be in the low nanomolar range to ensure that the experiments are performed at tracer dose. This was made possible because of the high specific radioactivities routinely obtained at the end of the radiosynthesis. Within the range of injected doses (0.01–0.08 nmol/kg body weight), the amount of mass injected did not influence the DV value, even in regions with a low nAChR density.

Since nicotinic receptors of the $\alpha_4\beta_2$ subtype are almost ubiquitous in the human brain (*26*), the definition of a reference region is not straightforward. Autoradiographic studies using ^{125}I-5I-A-85380 have demonstrated that the globus pallidus is almost devoid of nAChRs in humans (*27*). However, due to the finite resolution of PET systems, the activity measured in the globus pallidus (lying between the putamen and the thalamus) suffers from a spillover effect. Because a reliable segmentation method coupled to a partial-volume correction software is not yet available, this region was not explored as an area for a "zero-receptor region." Therefore, a noninvasive method for DV calculation using a reference region could not be applied to 2-^{18}F-fluoro-A-85380 PET data.

Previous studies in anesthetized monkeys (*9,28*) showed that 2-^{18}F-fluoro-A-85380 kinetics are slow and that a short scan duration could result in an underestimation of model parameters. However, a long scanning period is a drawback for patient studies. Therefore, the present study was designed to test whether a reliable quantification of 2-^{18}F-fluoro-A-85380 brain distribution in humans could be obtained in <4 h. Indeed, in the rhesus monkey, the underestimation of the DV, compared with 7-h reference values, was null in all regions at 4 h, except in the thalamus (*28*). In 2 other studies in humans, a 4-h experiment using ^{123}I-5I-A-85380 (*24*) or 6-^{18}F-fluoro-A-85380 (*25*) has been proposed to quantify nAChRs binding in all regions. Our study aimed at reducing the acquisition time, even at the expense of thalamic structures. The thalamus, though the richest in nicotinic receptors, is not the most relevant for clinical studies since degenerative diseases mainly affect the striatum (Parkinson's disease) or the hippocampus and cortex (Alzheimer's disease).

Because the subjects could not lie inside the scanner for 4 h, the PET acquisition was divided into 2 scans. The 2 scans were then coregistered with the MR scans to correct for differences in the position of the subject. To avoid contamination of the second transmission scan by the brain activity, the attenuation map was segmented (*15*), and the bias on the RA values induced by this segmentation was estimated at the end of the first scan.

Kinetic analysis of 2-^{18}F-fluoro-A-85380 brain uptake revealed that the 2TCM was more accurate than the 1TCM to describe PET data in all VOIs, indicating that the exchange between the tissue compartments cannot be considered as instantaneous. However, individual identification of each parameter of the 2TCM was not reliable and, therefore, only the DV could be estimated. Since the 1TCM and the 2TCM could provide an estimate of the DV with similar SDs, the 2TCM was chosen for its higher accuracy.

The second method tested was Logan graphical analysis (*13*), which allows one to compute the DV of reversible ligands. One advantage of this method is that it requires the estimation of only 1 parameter compared with 4 parameters for the 2TCM. The DV_{Logan} values obtained were slightly lower than the DV_{2TCM} values in all VOIs. This may be due to the noise-induced bias inherent to the Logan analysis (*29,30*).

The kinetic analysis and the Logan graphical analysis required similar study durations to provide stable results in all regions. For a given PET scan duration, the dispersion of the errors was lower with the kinetic analysis, indicating that this latter analysis is more precise.

CONCLUSION

2-^{18}F-Fluoro-A-85380 can be used to assess nAChR binding in the human brain with PET. After a bolus injec-

tion of the radiotracer, among the PET scan durations and the modeling strategies tested, a scanning time of 140 min and the 2TCM seem to represent a reliable method for estimating the regional distribution of nAChRs in neurodegenerative diseases.

ACKNOWLEDGMENTS

This work was supported in part by a grant from Janssen-Cilag France. Philippe Bouhours, MD, is gratefully acknowledged for his scientific support.

REFERENCES

1. Gotti C, Fornasari D, Clementi F. Human neuronal nicotinic receptors. *Prog Neurobiol.* 1997;53:199–237.
2. Court JA, Piggott MA, Lloyd S, et al. Nicotine binding in human striatum: elevation in schizophrenia and reductions in dementia with Lewy bodies, Parkinson's disease and Alzheimer's disease and in relation to neuroleptic medication. *Neuroscience.* 2000;98:79–87.
3. Khachaturian ZS, Radebaugh TS. Synthesis of critical topics in Alzheimer's disease. In: Khachaturian ZS, Radebaugh TS, eds. *Alzheimer's Disease: Cause(s), Diagnosis, Treatment and Care.* Boca Raton, FL: CRC Press; 1996: 3–25.
4. Koren AO, Horti AG, Mukhin AG, et al. 2-, 5-, and 6-Halo-3-(2(S)-azetidinylmethoxy)pyridines: synthesis, affinity for nicotinic acetylcholine receptors, and molecular modeling. *J Med Chem.* 1998;41:3690–3698.
5. Valette H, Bottlaender M, Dollé F, et al. Characterization of the nicotinic ligand 2-[^{18}F]fluoro-3-[2(S)-2-azetidinylmethoxy]pyridine in vivo. *Life Sci.* 1999;64: PL93–PL97.
6. Dollé F, Dolci L, Valette H, et al. Synthesis and nicotinic acetylcholine receptor in vivo binding properties of 2-fluoro-3-[2(S)-2-azetidinylmethoxy]pyridine: a new positron emission tomography ligand for nicotinic receptors. *J Med Chem.* 1999;42:2251–2259.
7. Sihver W, Nordberg A, Langstrom B, et al. Development of ligands for in vivo imaging of cerebral nicotinic receptors. *Behav Brain Res.* 2000;113:143–157.
8. Muzic RF Jr, Berridge MS, Friedland RP, Zhu N, Nelson AD. PET quantification of specific binding of carbon-11-nicotine in human brain. *J Nucl Med.* 1998;39: 2048–2054.
9. Valette H, Bottlaender M, Dolle F, et al. Imaging central nicotinic acetylcholine receptors in baboons with [^{18}F]fluoro-A-85380. *J Nucl Med.* 1999;40:1374–1380.
10. Ding YS, Molina PE, Fowler JS, et al. Comparative studies of epibatidine derivatives [^{18}F]NFEP and [^{18}F]N-methyl-NFEP: kinetics, nicotine effect, and toxicity. *Nucl Med Biol.* 1999;26:139–148.
11. Bottlaender M, Valette H, Roumenov D, et al. Biodistribution and radiation dosimetry of [^{18}F]fluoro-A-85380 in healthy volunteers. *J Nucl Med.* 2003;44: 596–601.
12. Valette H, Dollé F, Bottlaender M, Hinnen F, Marzin D. Fluoro-A-85380 demonstrated no mutagenic properties in in vivo rat micronucleus and Ames tests. *Nucl Med Biol.* 2002;29:849–853.
13. Logan J, Fowler JS, Volkow ND, et al. Graphical analysis of reversible radioligand binding from time-activity measurements applied to [N-^{11}C-methyl]-(-)-cocaine PET studies in human subjects. *J Cereb Blood Flow Metab.* 1990;10: 740–747.
14. Brix G, Zaers J, Adam LE, et al. Performance evaluation of a whole-body PET scanner using the NEMA protocol. *J Nucl Med.* 1997;38:1614–1623.
15. Xu M, Cutler PD, Luk WK. Adaptive segmented attenuation correction for whole body PET imaging. *IEEE Trans Nucl Sci.* 1996;43:331–336.
16. Viola P, Wells WM. Alignment by maximization of mutual information. *Int J Comput Vision.* 1997;24:137–154.
17. Leenders KL, Perani D, Lammertsma AA, et al. Cerebral blood flow, blood volume and oxygen utilization: normal values and effect of age. *Brain.* 1990; 113:27–47.
18. Koeppe RA, Holthoff VA, Frey KA, Kilbourn MR, Kuhl DE. Compartmental analysis of [^{11}C]flumazenil kinetics for the estimation of ligand transport rate and receptor distribution using positron emission tomography. *J Cereb Blood Flow Metab.* 1991;11:735–744.
19. Marquardt DW. An algorithm for least square estimation of nonlinear parameters. *SIAM J.* 1963;11:431–441.
20. Akaike H. A new look at the statistical model identification. *IEEE Trans Automat Contr.* 1974;AC19:716–723.
21. Carson RE. Parameters estimation in positron emission tomography. In: Phelps ME, Mazziota JC, Schelbert HR, eds. *Positron Emission Tomography: Principles Applications for the Brain and the Heart.* New York, NY: Raven Press; 1986: 347–390.
22. Adem A, Nordberg A, Jossan SS, Sara V, Gillberg PG. Quantitative autoradiography of nicotinic receptors in large cryosections of human brain hemispheres. *Neurosci Lett.* 1989;101:247–252.
23. Marutle A, Warpman U, Bogdanovic N, Nordberg A. Regional distribution of subtypes of nicotinic receptors in human brain and effect of aging studied by (±)-[^{3}H]epibatidine. *Brain Res.* 1998;801:143–149.
24. Fujita M, Ichise M, Van Dyck CH, et al. Quantification of nicotinic acetylcholine receptors in human brain using [^{123}I]5-I-A-85380 SPET. *Eur J Nucl Med Mol Imaging.* 2003;30:1620–1629.
25. Ding YS, Fowler JS, Logan J, et al. 6-[^{18}F]Fluoro-A-85380, a new PET tracer for the nicotinic acetylcholine receptor: studies in the human brain and in vivo demonstration of specific binding in white matter. *Synapse.* 2004;53:184–189.
26. Paterson D, Nordberg A. Neuronal nicotinic receptors in the human brain. *Prog Neurobiol.* 2000;61:75–111.
27. Pimlott SL, Piggott M, Owens J, et al. Nicotinic acetylcholine receptor distribution in Alzheimer's disease, dementia with Lewy bodies, Parkinson's disease, and vascular dementia: in vitro binding study using 5-[^{125}I]-A-85380. *Neuropsychopharmacology.* 2004;29:108–116.
28. Chefer SI, London ED, Koren AO, et al. Graphical analysis of 2-[^{18}F]FA binding to nicotinic acetylcholine receptors in rhesus monkey brain. *Synapse.* 2003;48: 25–34.
29. Feng D, Wang Z, Huang SC. A study on statistically reliable and computationally efficient algorithms for generating local cerebral blood flow parametric images with positron emission tomography. *IEEE Trans Med Imaging.* 1993;12:182–188.
30. Slifstein M, Laruelle M. Effects of statistical noise on graphic analysis of PET neuroreceptor studies. *J Nucl Med.* 2000;41:2083–2088.